PERFORMANCE OF AN ELECTROMAGNETIC BEARING FOR THE VIBRATION CONTROL OF A SUPERCRITICAL SHAFT*

C.D. Bradfield, J.B. Roberts, and R. Karunendiran
University of Sussex
Falmer, Brighton, England

The flexural vibrations of a rotating shaft, running through one or more critical speeds, can be reduced to an acceptably low level by applying suitable control forces at an intermediate span position. If electromagnets are used to produce the control forces then it is possible to implement a wide variety of control strategies.

A test rig is described which includes a microprocessor-based controller, in which such strategies can be realised in terms of software-based algorithms. The electromagnet configuration and the method of stabilising the electromagnet force-gap characteristic are discussed. The bounds on the performance of the system are defined. A simple control algorithm is outlined, where the control forces are proportional to the measured displacement and velocity at a single point on the shaft span; in this case the electromagnet behaves in a similar manner to that of a parallel combination of a linear spring and damper. Experimental and predicted performance of the system are compared, for this type of control, where various programmable rates of damping are applied.

INTRODUCTION

In many engineering applications it is desirable to control the amplitude of transverse vibrations of flexible transmission shafts, especially if the design speed range encompasses one or more critical speeds. It can be demonstrated theoretically (e.g. see Refs.1 to 3) that it is possible to satisfactorily control the flexural vibrations of a rotating shaft by applying control forces at a single intermediate span position. If the position of the control force application is suitably chosen then satisfactory reductions in the amplitude of vibration may be achieved over a speed range covering several critical speeds.

Two control devices, which are appropriate for this application, have been investigated in recent years - the squeeze-film bearing (e.g. see Refs. 4 and 5) and the electromagnetic bearing. The former has proved a relatively robust and reliable means of achieving vibration control. However, despite considerable efforts, it has proved difficult to predict its dynamic performance quantitatively, with any degree of accuracy.

---

* This work was supported by the Science and Engineering Research Council. The authors gratefully acknowledge this source of funding.

Electromagnetic bearings offer an attractive alternative approach and interest in such devices, as a means of active vibration control, has grown rapidly during the last few years [6-11]. The considerable advantage of such bearings is that it is possible to implement a wide variety of control strategies, particularly if they are operated under computer control. Moreover, it is possible, at least in principle, to predict their dynamic characteristics fairly accurately. This implies that it should be possible to design an electromagnetic control device which has a quantitatively predictable performance when applied to any particular rotor-bearing system.

Various types of electromagnetic control device have been described in the literature [6-11]. One of the simplest, and most promising, of such devices comprises six pole pieces surrounding the shaft, with three alternate energised poles. With this arrangement, combined with microprocessor control, it has been demonstrated experimentally that it is possible to control a rotating shaft satisfactorily, when it passes through critical speeds [11]. However, a quantitative comparison between experimental and predicted performance of the combined rotor-electromagnet system was not attempted in this earlier work.

In the present paper the rationale behind the adoption of this particular electromagnet configuration is initially discussed. This is followed by a description of the power electronics, and microprocessor-based control system used to drive the electromagnets, with emphasis on the factors which limit the performance of the system. The implementation of a simple control strategy, in which the electromagnet behaves approximately as a linear spring-plus-damper, is outlined and it demonstrated theoretically that, with this form of control, the complete rotor-electromagnet system can become unstable, under certain circumstances. A qualitative prediction of the influence of various factors on stability is obtained from this theory, which is fully in accord with experimental observations.

The paper concludes with some experimental results obtained from a test rig, in which the rotor is a simple shaft, of uniform cross-section, and the only source of excitation, when rotating, is the initial bend. For pure damping control, the results of free-decay tests are shown, which clearly demonstrate the effect of increasing the programmable rate of damping. A parametric identification technique, applied to the free-decay data, results in a direct calibration of the relevant damping coefficient. Results obtained from the test rig, when the shaft is rotating under damping control, are then presented and compared with corresponding theoretical predictions, for a speed range covering the first critical speed of the shaft.

EQUIPMENT

Rotor-Bearing System

The experimental rotor configuration is shown in Fig.1 and comprises a 25 mm diameter shaft of austenitic stainless steel, mounted in self-aligning ball races, giving a length between bearings of 1500 mm. The shaft is driven through a light flexible coupling, and can be driven at up to 6000 r.p.m. from a variable speed drive.

In this configuration, the first two critical speeds are 1260 and 5480 r.p.m. Additional masses may be added to bring the third critical speed within the design maximum speed. The active element used to control shaft motions, the electromagnet assembly, is located at the one-sixth span point, and can thus apply forces which are effective in controlling motions in at least the first three modes.

The shaft position is measured using capacitative transducers, which operate reliably in the magnetic fields encountered. These transducers operate satisfactorily as they are not subjected to oil contamination. Commercial equipment is used to energise the transducers and to demodulate their outputs. Transducers are mounted horizontally and vertically, and measure these components of shaft motion at two points, located between the magnet and the centre of the rotor.

Electromagnet Configuration

The active control element is shown in Fig.2 and comprises six pole pieces surrounding the shaft, with three alternate poles wound, and the three interleaved poles unenergised. The flux paths pass through the poles and their backing ring, through the small airgaps, and through a cylindrical core 50.8 mm diameter mounted on the shaft. This configuration gives radial fluxpaths in the central core and simplifies its construction, thin laminations being used to limit eddy current losses.

Design of the electromagnets is dominated by the need to linearise forces as the airgaps change. The attractive force F across an airgap is related to flux density B by the square-law relation $F = B^2 a/2\mu_o$, where a is the poleface area and μ_o the permeability of free space ($= 4\pi \times 10^{-7}$ H/m). The flux density is proportional to current I, but inversely proportional to the total air-gap g. Neglecting leakage flux and working below saturation, $B = \mu_o NI/g$ where N is the number of turns. An electromagnet thus produces forces which vary as $1/g^2$. At small gaps the rotor plus electromagnet will be unstable. To stabilise and linearise this behaviour, Salm and Schweitzer [9] have described an electromagnetic actuator in which each electromagnet coil contains two windings, carrying a bias current I_o, and a control current I. A pair of electromagnets on opposite sides of the core are connected such that flux on one electro-magnet is proportional to $I_o + I$, while the opposite electromagnet produces flux proportional to $I_o - I$. This system can be shown to linearise first order response only, with respect to both I and g. The system has a high steady power dissipation due to the bias currents I_o, and requires a unidirectional power amplifier (for bias current) and one bidirectional power amplifier per pair of electromagnets.

We have chosen instead to follow previous work on electromagnetic suspensions at Sussex [12], and control flux densities directly. Hall-effect plates are installed in the airgap at the centre of each energised pole to measure flux densities here. The electromagnets and their power amplifiers lie within an inner feedback loop, where the measured flux is compared with the drive signal, which is thus a flux demand. The non-linearity with respect to electromagnet gap is thereby

removed. The Hall plates are 0.35 mm thick. They, and their mechanical protection, require a small increase in airgap.

The control system has been implemented under microprocessor control in order to develop sophisticated control strategies. At this point it is only necessary to note that complex drive waveforms can be readily generated. It is no longer necessary to obtain the linear characteristic which differential driving of a pair of opposed electromagnets can give. The minimum provision of electromagnets and their drive amplifiers can be re-examined.

The requirement is to control two degrees of freedom of shaft motion of the electromagnet location, using devices which can apply attractive forces only. For any n degrees of freedom considered together, the minimum number of electromagnets will be n+1, if a suitable geometry is chosen. The one additional electromagnet arises from the restriction to attractive forces. It can be best visualised by considering the suspension to require one indeterminacy, allowing (though not requiring) all magnets to be preloaded, with a set of self-equilibrating forces. Having provided this system any direction of resultant force can be generated by suitable matched changes in the magnet forces. Operation is, however, not restricted to this fully biased mode, and minimum power dissipation is obtained if bias is reduced until the first magnet drops to zero force.

It may be noted that this principle differs slightly from electromagnetic suspensions, in which the weight of an object may often be used to preload the system of electromagnets, which can then be reduced in number by one. Without this modification it is indeed possible to identify a system of 7 electromagnets which can apply all 6 independent force components to a platform.

If the two translational degrees of freedom of the shaft at the electromagnet location are considered separately, then two attractive forces are required to control each. The total requirement is four electromagnets and drive amplifiers, and there is little economy over previous systems. However, taking the two degrees of freedom together, three electromagnets, each with its drive amplifer, are sufficient. This offers considerable economies in power amplifiers, and simplifications in the packing of coils and poles in the electromagnet assembly. This configuration, shown in Fig.2, is used in the present work. Unwound poles are placed between each of the wound poles with a single backing ring. The layout ensures that only unidirectional current drive to each coil is required; this considerably simplifies the power amplifier design.

Power Electronics and Control

Each electromagnet coil is energised by a power amplifier of the pulse-width modulation (p.w.m.) type. The connections of the coil to the d.c. power supply of voltage V_s are switched to alternately drive increases and decreases in the coil current.

The switching frequency is high compared with the coil time constant L/R, and is normally above the audible frequency range. The

input voltage to the amplifier sets the mark/space ratio of the switching signal. The on-time t_1 as a fraction of the total period τ is related to the current I, averaged over the switching cycle by:

$$t_1/\tau = \tfrac{1}{2} + (1/2V_S)((LdI/dt) + 2E + IR) \qquad (1)$$

where E is the back-emf generated by the core velocity.

The block diagram of the control system is shown in Fig.3. The outputs of the equipment energising the displacement transducers are used directly as the displacement signals. They are also bandwidth limited and passed through analogue differentiators to give the velocity signals. The signals pass through sample and hold gates, and can be switched onto two 12-bit successive approximation analogue-to-digital converters. These are interfaced to the Z8002 microprocessor over the Z-bus. Outputs from the microprocessor are provided through 12-bit digital-to-analogue converters which drive the flux error amplifiers. Timing and shaft-speed measurement are driven through counter-timers.

As a prototype system, the Z8002 is mounted in a development module containing the monitor and a large area of random-access memory (RAM). The system is commanded from a terminal, and program editing, storage and assembly is carried out on a host system running under CP/M. Machine code programs are downloaded into the development module's RAM in order to operate the system. A production version would omit terminal and host system, and store the fixed program in ROM on the microprocessor system, with automatic initialisation and execution on reset as power is first applied.

The Z8000 series processor was selected for the project, as the only 16 bit processor available in the U.K. at the time the project started.

Software

The microprocessor software was developed using the Z8000 assembly language, and is required to operate at two levels. At the low level, for a high computation speed, a loop is executed, initiated by a timer which sets the 550 μs sampling rate. The sample-and-hold gates, multiplexors and ADC's are controlled to measure the shaft position and velocity in x- and y-directions, and these values are stored. The control forces are computed, and resolved onto the magnet directions. As the outputs are used as a flux demand, it is necessary to perform a square root extraction: this is performed as a direct look-up in a 4K word table. Finally the control signals are output through the DAC's.

At a higher, and slower, level the constants in the control law may be altered, in response to measurements of shaft speed or to observed performance. This level is performed in the processor's normal mode, and the low level tasks described above, and speed measurement, are initiated by vectored interrupts, which enter the processor's system mode and initiate these tasks as the appropriate interrupt service routines.

The results described below were obtained using an earlier development version of the software in which the higher software level is not implemented.

CHARACTERISTICS OF THE ELECTROMAGNET SYSTEM

Force Resolution

The electromagnet system is normally required to generated rotating forces which are synchronous with the rotor. In this mode, the required forces in x- and y-directions are computed as F_x and F_y, and the required forces in the three electromagnets are obtained as shown in Fig.4. For any direction of the resultant of F_x and F_y, one magnet can generate forces opposing the resultant, and it is reduced to the set minimum force F_o. The axes of the two magnets which are driven include the direction of the resultant.

The resolution is simple to program, and a pseudo-code for this is given in Appendix A. This gives the derivation of the required magnet forces F_1, F_2, F_3 in terms of the computed forces F_x,F_y. Addition of a minimum force F_o is included within the table look-up, which will be performed after execution of this code, to obtain the drive voltages to the power amplifiers.

Low Frequency Performance

At low frequencies, the capacity of the electromagnet system is limited by core saturation, and by coil dissipation. The shaft speeds are high compared with the coil thermal time constants. Mean power dissipation, rather than maximum instantaneous dissipation, will produce this limit. At constant air-gap, this mean dissipation is proportional to the area under the force waveform, but in general the currents are modulated by airgap variations.

High Frequency Performance

The p.w.m. amplifier open loop conductance was shown to vary with the signal frequency. The e.m.f. E is generally small, and the gain shows a first-order response

$$\frac{I}{t_1/\tau} = \frac{2V_s/R}{1 + j\omega/\omega_o} \qquad (2)$$

where the corner frequency ω_o is the inverse of the coil time constant L/R. This is the longest and dominant time constant in the system, and imposes severe performance limitations. The flux feedback loop operates to reduce gain but also increases the corner frequency, multiplying it by the loop gain. At the closed-loop corner frequency, substantial phase errors occur, as the amplifier contributes a 45^o phase lag. Small contributions may be introduced elsewhere in the loop, as substantial filtering must be introduced at the p.w.m. switching frequency.

A further limitation arises when slew-rate limiting occurs. At low currents dI/dt cannot exceed $\pm V_S/L$. This imposes a limiting linear rise or fall of current with time, and hence a parabolic limiting force-time curve. The force-time waveform for one magnet is shown in Fig.5.

A limiting slew-rate condition is shown by the broken line which at zero force is horizontal. For a zero bias level, i.e. $F_O = 0$, it will be seen that the initial rise in the force waveform can never be attained, and distortion will occur. A small bias level is of great benefit in allowing a useful rate-of-rise of current to be attained at point B. This also avoids operation conditions for the p.w.m. amplifiers at which commutation times become significant.

In operation, the choice lies between accepting a small distortion when a small bias level is used, and eliminating distortion but substantially increasing dissipation by adopting a high bias level. The former option is preferred at present.

The operating area of the power amplifier-electromagnet combination is shown in Fig.6. Further investigation shows that only the dissipation limit alters as the core moves within the magnet poles.

The magnet used in the present work is designed to produce 400 N at up to 100 Hz, using a 320 volt supply, within acceptable distortion limits.

CONTROL STRATEGY

In the present work the control strategy is to provide control forces which depend on the measured motion of the shaft, at one span position only. Since the shaft-bearing system under consideration is symmetrical, one need only describe the strategy for a single plane of vibration.

Suppose that the transverse displacement of the shaft is measured at a distance, x_m, from one end, and that the control force is applied at a distance, x_C, from the same end. Let $F_C(t)$ denote the time varying control force, and y_m be the measured displacement.

One of the simplest approaches, and that adopted here, is to generate a control force which is a linear combination of a displacement-proportional component and a velocity-proportional component, i.e.

$$F_C = -ky_m - c\dot{y}_m \qquad (3)$$

where k is a "spring" constant and c is a "damping" constant. When x_m and x_C are equal the constants k and c have their usual meaning. In the present application the shaft vibrates synchronously - i.e. y_m (and $\dot{y}_m$) fluctuate harmonically, with a frequency equal to the shaft's rotational speed, ω. It follows, from equation (3) that $F_C(t)$ is also harmonic.

If k and c are allowed to vary with ω than one can achieve "optimum" control, over any required speed range [3]. However, in the present investigation attention is focussed on the situation where both k and c are constant, independent of speed. As theoretical work has demonstrated, if k and c are chosen carefully, this type of control can successfully limit vibration amplitudes over a speed range covering several critical speeds [2].

THEORETICAL TREATMENT

Modelling the Shaft-Bearing System

To obtain theoretical predictions of the shaft vibrational behaviour, when controlled by a force, as given by equation (3), a computer program was written, based on the stiffness method. The shaft was discretised into a number of lumped masses, with the elastic segments between these masses being taken to be massless. The bearings were modelled as simple, pinned supports. The program could cater for any form of excitation, arising from the initial bend of the shaft, and the distribution of mass unbalance.

The equations of motion were formulated in the standard form

$$\underset{\sim}{m}\,\ddot{\underset{\sim}{y}} + \underset{\sim}{c}\,\dot{\underset{\sim}{y}} + \underset{\sim}{K}\,\underset{\sim}{y} = \underset{\sim}{Q}(t) \qquad (4)$$

where $\underset{\sim}{m}$, $\underset{\sim}{c}$ and $\underset{\sim}{K}$ are the mass, damping and stifness matrices, respectively, $\underset{\sim}{y}$ is a column of displacements and $\underset{\sim}{Q}(t)$ is a column of excitation components. A numerical solution of equation (4) enabled the vibration amplitudes of the discrete masses, at any rotational speed, to be calculated. Moreover, the stability of the system could be assessed, through an eigenvalue analysis of the homogeneous form of equation (4) ($Q(t) = 0$).

Approximate Analysis for Damping Control

If attention is focussed on a speed range covering the first critical speed only, and damping control alone is considered, then it is possible to obtain a simple analytical expression for the vibration response. This expression is likely to be fairly accurate in the case of the present shaft, since its natural frequencies are well separated.

Considering initially, for simplicity, the case of free vibration (i.e. no rotation) one can approximate vibration in the first mode by assuming that it is of the same form as undamped vibration - i.e.,

$$y(x,t) = Y(t) \sin \left(\frac{\pi x}{\ell}\right) \qquad (5)$$

where y, as before denotes transverse displacement, Y(t) is a function of time only and ℓ is the total shaft length. A single degree of freedom equation of motion can then be formulated using the energy relationship

Rate of change of total energy = - Rate of energy dissipation
(potential + kinetic) due to damping (6)
This leads (see Appendix B) to the equation

$$\ddot{y} + \beta\dot{y} + y = 0 \tag{7}$$

where here differentiation is with respect to the non-dimensional time

$$\tau = \omega_1 t \tag{8}$$

and ω_1 is the first natural frequency of the shaft. β, a non-dimensional damping coefficient is related to c (see equation (3)) through the equation

$$\beta = \frac{2c}{M\omega_1} \sin\left(\frac{\pi x_m}{\ell}\right) \sin\left(\frac{\pi x_c}{\ell}\right) \tag{9}$$

where M is the total mass of the shaft. In the experiments to be discussed later $x_m/\ell = 1/3$ and $x_c/\ell = 1/6$; hence, in this particular case,

$$\beta = \frac{\sqrt{3}c}{2M\omega_1} \tag{10}$$

For the case of a rotating shaft, with initial bend excitation only, equation (7) can be generalised by incorporating a non-zero right-hand side. If the initial bend is assumed to approximate to the shape of a half-sine wave then, at any shaft location, x, one finds, approximately, that

$$\ddot{y} + \beta\dot{y} + y = b \cos \omega t \tag{11}$$

where b is the initial bend at that location. Solving equation (11) for synchronous vibration shows that the amplitude of vibration, A, at location x, is given by

$$\frac{A}{b} = \left[\frac{1}{(1-\Omega^2)^2+\beta^2\Omega^2}\right]^{1/2} \tag{12}$$

where

$$\Omega = \omega/\omega_1 \tag{13}$$

is a non-dimensional frequency.

Comparisons between predictions from equation (12), and the more accurate numerical approach described earlier, generally showed good agreement. Fig.7 shows a typical comparison for the case where c = 272

Ns/m. Here the amplitude of vibration, in one plane, at the damper position is plotted against rotational speed.

Stability Considerations

The ideal control law expressed by equation (3) can only be realised approximately, in practice. Due to the hardware limitations described earlier, the bandwidth of the electromagnetic system (EMS) is of order 100 Hz; at frequencies in excess of this the phase shifts and gain variations associated with the EMS become very significant and must be taken into account in any assessment of the overall stability of the total shaft-plus-EMS.

The total system may be regarded as two sub-systems - the shaft-bearing system (SBS) and the electromagnetic system (EMS). These sub-systems are coupled through the following two variables:

(i) the force $F_c(t)$, at position x_c
(ii) the shaft displacement, $y_m(t)$ at position x_m.

The appropriate block diagram representation of the total system is shown in Fig.8. For a stability assessment it is sufficient to consider the case of no rotation - i.e., no excitation, and motion in one plane only.

For the SBS, the Laplace transform of $y_m(t)$, denoted $Y_m(s)$, is related to the Laplace transform of $F_c(t)$, denoted $F_c(s)$, though the linear relationship

$$F_c(s) = M(s)Y_m(s) \tag{14}$$

Here M(s) is the "mechanical" transfer function for the shaft-bearing system. Similarly, for the EMS one can write (assuming that this sub-system behaves, at least approximately, in a linear fashion)

$$F_c(s) = E(s)Y_m(s) \tag{15}$$

where E(s) is the "electrical" transfer function. Eliminating $F_c(s)$ between equations (14) and (15) one finds that

$$D(s)Y_m(s) = 0 \tag{16}$$

where

$$D(s) = M(s) + \bar{E}(s) \tag{17}$$

and

$$\bar{E}(s) = -E(s) \tag{18}$$

The total systems characteristic equation is thus

$$D(s) = 0 \tag{19}$$

For stability all the roots of equation (18) must lie on the left hand side of the complex s-plane. The position of these roots can be determined numerically if both M(s) and E(s) can be expressed in algebraic form. Alternatively, a graphical procedure can be used.

In the present paper the graphical technique known as the Leonhard Locus (e.g. see Ref.13) will be used to examine the factors which influence total system stability. This involves a consideration of the mapping between the s-plane and the complex D-plane, where D is defined by equation (17). Firstly, it may be observed that the roots of the characteristic equation all map to the origin of the D-plane. Now if a point travels along the imaginary axis of the s-plane - i.e., $s = j\omega$, with ω increasing from $\omega = 0$ - it will map to a curved locus, $D(j\omega)$, in the D plane, known as the Leonhard Locus. In the case of a stable system all the roots in the s-plane lie to the left-hand side of the locus $s = j\omega$; this implies that the mapped, Leonhard locus, in the D-plane will be such that the origin will always lie on the left hand side, to an "observer" travelling along the locus in the direction of increasing frequency, ω. For a system at the threshold of stability the Leonhard locus should pass exactly through the origin of the D-plane.

In the present case the Leonhard locii, $M(j\omega)$ and $E(j\omega)$, may be evaluated separately and then combined, through a simple addition. According to equation (17) the combined Leonhard locus is given by

$$D(j\omega) = M(j\omega) + \overline{E}(j\omega) \tag{20}$$

Now $M(j\omega)$ and $\overline{E}(j\omega)$ are directly related to the frequency response functions for the mechanical and electrical sub-systems, respectively. Thus the stability of the total system can be deduced directly from the characteristics (amplitude and phase variation with frequency) of these two functions.

For a pinned-pinned uniform shaft the appropriate frequency response function, $M(j\omega)$, can be found by standard methods. If it is assumed that the introduction of structural damping does not lead to coupling between the modes then a modal expansion for the inverse of $M(j\omega)$ is as follows:

$$\frac{1}{M(j\omega)} = \sum_{n=1}^{\infty} \frac{\alpha_n}{[\omega_n^2 + (j\omega)^2 + 2(j\omega)\varsigma_n\omega_n]} \tag{21}$$

where

$$\omega_n = n^2\pi^2 \frac{EI}{\ell^4} \tag{22}$$

is the nth natural frequency, E is Young's modulus for the shaft material, $I = \pi d^4/64$, where d is the shaft diameter, and m is the mass per unit length of the shaft. ς_n ($n = 1,2...$) are the modal damping factors and the coefficients α_n are given by

$$\alpha_n = \frac{2}{m\ell} \sin\left(\frac{n\pi x_m}{\ell}\right) \sin\left(\frac{n\pi x_c}{\ell}\right) \tag{23}$$

Fig. 9 indicates the general behaviour of the Leonhard locus, $M(j\omega)$, for the first three modes. The arrows indicate the direction of increasing frequency. It is noted that there is one "branch" of the locus, corresponding to each mode; the n^{th} branch intersects the imaginary axis of the $M(j\omega)$ plane at $\omega \sim \omega_n$. The height of such an intersection is, to a good approximation, directly proportional to the structural damping of the corresponding mode. In general the structural damping will become more effective as the mode number, n, increases; this is one reason why the branches of $M(j\omega)$ become progressively higher, as Fig.9(a) indicates. For an imaginary observer moving along any particular branch the origin always appears to the left hand side - it follows that the mechanical sub-system, considered in isolation, is always stable.

For the "ideal" control law given by equation (3) the corresponding Leonhard locus $\bar{E}(j\omega)$ is easily found to be

$$\bar{E}(j\omega) = k + (j\omega)c \qquad (24)$$

This locus is sketched in Fig. 9(b). It is evident that a combination of $M(j\omega)$ and $\bar{E}(j\omega)$ will lead to a total system locus, $D(j\omega)$ which also satisfies the graphical stability criterion.

The main interest here concerns the effect of the electromagnet system's non-ideal characteristic on the total system stability. Figs. 10(a) and (b) show, qualitatively, the difference between the ideal pure spring, and the ideal pure damper, $\bar{E}(j\omega)$ loci, respectively, and the corresponding loci of the kind obtained in practice. As ω increases, the phase shifts, and gain reduction, becomes progressively more significant, resulting in curved loci.

A combination of $M(j\omega)$ with the actual $E(j\omega)$ can lead to a Leonhard locus which indicates instability. This is illustrated in Fig.11. If a particular branch of the $M(j\omega)$ is "pulled" below the origin, through the addition of $\bar{E}(j\omega)$, then total system instability is indicated. The threshold of instability occurs, for a particular mode, when the relevant branch of the combined locus <u>just</u> passes through the origin.

Let s denote distance travelled along a Leonhard locus. Then it may be observed that $ds/d\omega$ for $M(j\omega)$, in the vicinity of a natural frequency, is normally much greater than the corresponding rate of change for $\bar{E}(j\omega)$. Also, for $\omega = \omega_n$, $M(j\omega_n)$ is, to a close approximation, entirely imaginary, with a value given by (from equation (21))

$$M(j\omega_n) = j.\frac{2\zeta_n\omega_n^2}{\alpha_n} \qquad (25)$$

This result follows from the fact that the contribution to $M(j\omega_n)$ from the n^{th} mode is dominant. If the combination of $M(j\omega)$ and $\bar{E}(j\omega)$ is to result in a locus which passes above the origin then one requires, approximately, that

$$\frac{2\varsigma_n\omega_n^2}{\alpha_n} + \mathrm{Im}(\bar{E}(j\omega_n)) > 0 \qquad (26)$$

This condition gives a criterion for "stability in the n^{th} node". Total stability obviously requires that inequality (26) be satisfied for all n.

Several conclusions can be drawn from this stability criterion. Firstly, considering the case of pure stifness control, it is evident that, since ς_n are generally very small quantities ($\varsigma_n \ll 1$), very small phase shifts can result in instability (see Fig.10(b)). Thus this method of control is very prone to instability problems.

In considering the other extreme case of pure damping control it is convenient to represent $\bar{E}(j\omega)$ as

$$\bar{E}(j\omega) = j\omega c\, E_A e^{-j\Phi} \qquad (27)$$

Evidently, for ideal damping $E_A = 1$, $\Phi = 0$ and, from inequality (26), stability is assumed, for all n. However, if $90^o < \Phi < 270^o$, at a particular natural frequency, ω_n, then the corresponding mode can become unstable. The critical value of damping coefficient, c^*, at which the n^{th} mode is marginally stable is given by (for $90^o < \Phi < 270^o$)

$$c^* = \frac{2\varsigma_n\omega_n}{E_A\alpha_n|\cos\Phi|} \qquad (28)$$

Again, since ς_n are usually very small compared with unity, c^* can be very low. It follows from equation (28) that improvements in the stable range of damping coefficient can be achieved by
(i) reducing the absolute value of cos Φ
(ii) reducing the non-dimensional gain, E_A
(iii) reducing the value of α_n, by repositioning the measuring location, x_m.

It is noted that, if only one mode of vibration is unstable, this instability can be removed, theoretically, by locating the measuring point at a node of that particular mode. This has the effect of making $\alpha_n = 0$, since the n^{th} mode has the mode shape sin ($n\pi x/\ell$) (see equation (23)).

COMPARISON BETWEEN THEORY AND EXPERIMENT

Results will now be presented which relate to the case of nominally pure damping (i.e. k = 0 in equation (3)).

Stability Observations

With $x_c = \ell/6$, and x_m close to x_c, experiments revealed that the shaft became unstable when the damping coefficient exceeded a small, non-zero level. The self-excitation was in the form of vibration in the third mode.

Referring to equation (28) one can conclude that, for the third mode, the value of c^* is very low. This is mainly due to the value of ϕ at $\omega 3$ ($\sim$ 180 Hz), which is in excess of 90^o. It was found experimentally that c^* could be increased by moving the measurement position closer to a node position of the third mode ($x_m = \ell/3$). This observation is in qualitative agreement with equation (28). It was also found experimentally that c^* could be increased by reducing the value of ϕ at ω_3, through modifications to the electronics and software. This again is in accord with equation (28).

To enable results to be obtained over a wide range of damping coefficient (c) values, the measuring point was located at a third mode node - i.e. at $x_m = \ell/3$. The total system was then found to be stable for c values up to about 700 Ns/m.

Free Decay Tests

Experimental estimates of the damping coefficient β, in equation (7), were obtained by performing free-decay tests on the non-rotating shaft. The shaft was pulled at its centre, through a small displacement, and then released. The subsequent transient decay was then recorded digitally, at equi-spaced time intervals, for various levels of damping coefficient.

Figs. 12(a) and (b) show typical free-decay experimental results, including the case where the electromagnetic damping is zero (i.e. structural damping only is present). The results were obtained for various programmable rates of damping by varying the rate constants (in arbitrary units) in the control program. To reduce the effects of noise, each of the free-decay results was obtained by averaging ten separate, individual results, obtained under identical conditions.

Each averaged free-decay result was processed by a parametric identification procedure, which fitted the experimental data to the solution of the following equation of motion, in a least-square sense [14,15];

$$\ddot{y} + \beta\dot{y} + \gamma y = 0 \qquad (29)$$

Figs.12 show comparisons between the solutions to equation (29) and the experimental data, where the theory is computed from the best fit values of β and γ. In every case a very good degree of fit is achieved. Table 1 summarises the results obtained for β and γ.

It is noted that γ is close to unity, as one would expect, for pure damping. Moreover, β is, to a very close approximation, proportional to the programmable damping rate, as Fig.13 shows. The results also show that the contribution of structural damping can be neglected.

Table 1

Programmable damping rate (arbitrary units)	estimated parameters β	γ
0	0.013	1.00
199	0.123	0.08
272	0.178	1.01
397	0.279	1.02
496	0.357	1.08
595	0.407	1.12
744	0.501	1.08

It can be concluded, from the analysis of these tests, that the electromagnetic control system performs as expected, at least for frequencies in the vicinity of the shafts first natural frequency (~ 21 Hz).

Rotating Shaft Results

For rotational speeds in the range 200 to 2500 r.p.m., the shaft's amplitude of vibration, in a single plane, was measured and plotted against shaft speed. The measurement location was at $x \sim \ell/6$; close to the magnet position. Figs. 14 show some typical comparisons between the experimental variations of vibration amplitude with rotational speed, and corresponding theoretical predictions, for two levels of damping. The theoretical predictions were obtained from the lumped-mass computer program, with damping values deduced from the β values found in the free-decay tests, using equation (10) to convert β to the damping coefficient c. The initial bend of the shaft was measured experimentally and used as input data for the program. Generally the degree of agreement between theory and experiment is very satisfactory, and it is evident that the vibration amplitude at the first critical speed can be controlled very satisfactorily by the electromagnet system. It is interesting to note that there is some variation in the experimental results, at each level of damping. Thus, the variation of amplitude with speed as the speed increased from zero to its maximum value (labelled 'before'), was found to differ somewhat from the corresponding variation as the speed decreased to zero (labelled 'after'). Further traverses in speed were found to produce further variations. This phenomenon is attributed to variations in the initial bend of the shaft, as the results of stress cycling. This effect has been observed in earlier investigations (e.g. see Ref.2). Measurements of the initial bend confirmed that it changed, as the results of a sequence of rotational tests. The initial bend was found to return to its original shape over a time period of order one day.

A direct estimate of the non-dimensional damping parameter β, produced by the electromagnet system, can be found by using the simple approximate result given by equation (12). In particular, at $\Omega = 1$ one has, from this equation,

$$A/b = 1/\beta \qquad (30)$$

Thus, taking the average of the experimental results, at each damping level, and dividing the amplitude of vibration at $\omega = 0(b)$ by the amplitude of vibration at $\omega = \omega_1$, one obtains a simple estimate of β. In Fig.15 the estimates of β, obtained in this way, are plotted against the corresponding estimates obtained from the analysis of the transient data. Each point here relates to one programmable rate of damping. The points lie very close to a straight line, at 45^o to the horizontal, showing a good degree of correlation. There is a small offset, which indicates that, in the case of rotation, there is a small additional contribution to the total damping. This contribution probably originates in the bearings. When allowance is made for this effect one can conclude, from Fig.15, that the test results obtained with the rotating shaft are in complete accord with the transient test results.

CONCLUSIONS

A microprocessor based electromagnet system for controlling the vibration of rotating flexible shafts has been described, and bounds on the performance of the system have been defined. Theoretical arguments have shown that, as a result of limitations to the performance of the electromagnet system, the complete shaft-plus-electromagnet system can become unstable under certain conditions. A simple stability criterion has been established which reveals the influence of various factors on stability. For the case where the electromagnet is programmed to behave as a simple damper, good agreement between experimental observations and theoretical predictions has been achieved, over a rotational speed range encompassing the shaft's first critical speed.

APPENDIX A

ALGORITHM FOR FORCE COMPONENT EVALUATION

```
fx :=      (required forces)
fy :=      (                )
fx':= fx/√3

if fx'>0 then
   if fx'>fy then
      call m3off
   else
     call m1off
else
   if -fx'>fy then
   call m2off
  else
      call m1off
endif

procedure m1off
 f2 := fx' + fy
 f3 :=-fx' + fy
 f1 := 0
endproc
```

```
procedure m2off
  f1 := -fx' - fy
  f2 :=  0
  f3 := -2*fx'
endproc

procedure m3off
  f1 := fx' - fy
  f2 := 2*fx'
  f3 := 0
endproc
```

APPENDIX B
APPROXIMATE EQUATION FOR FIRST MODE FREE VIBRATION WITH DAMPING

For a uniform shaft with pinned supports, free undamped vibration takes the form

$$y(x,t) = Y(t) \sin (\pi x/\ell) \tag{A1}$$

where Y(t) is a function of time only. A good approximation, when damping is applied through the electromagnets, is to assume that this basic form of vibration is still applicable. This approximation clearly will be most accurate when the damping is light.

The total kinetic energy of the vibrating shaft is then given by

$$KE = \frac{1}{2} \int_o^\ell my^2 dx \tag{A2}$$

where m is the mass per unit length. Combining equations (A1) and (A2) one finds that

$$KE = \frac{1}{4} MY^2 \tag{A3}$$

where $M = m\ell$. The total potential energy, in the form of elastic strain energy in the shaft, can also be easily calculated; thus

$$PE = \frac{EI}{2} \int_o^\ell \left(\frac{d^2y}{dx^2}\right)^2 dx \tag{A4}$$

and, from equations (A1) and (A4),

$$PE = \frac{EI\ \pi^4 Y^2}{4\ell^3} \tag{A5}$$

Finally, the rate of energy dissipation, R, is given simply by

$$\begin{aligned} R &= \text{Damper force x velocity at damper} \\ &= c y_m y_c \end{aligned} \tag{A6}$$

where y_c is the velocity at the electromagnet position and y_m is the velocity at the measuring point. From equations (A1) and (A6) one has

$$R = cY^2 \sin\left(\frac{\pi x_m}{\ell}\right) \sin\left(\frac{\pi x_c}{\ell}\right) \qquad \text{(A7)}$$

Now, following the energy relationship expressed by equation (6), one has

$$\frac{d}{dt}(PE + KE) = -R \qquad \text{(A8)}$$

Hence, from equations (A3), (A5) and (A7), one obtains a single degree of freedom equation of motion, as follows:

$$\frac{1}{2} M \ddot{Y} + \frac{cY}{2} \sin\left(\frac{\pi x_m}{\ell}\right) \sin\left(\frac{\pi x_c}{\ell}\right) + \frac{EI\,\pi^4}{2\ell^3} Y = 0 \qquad \text{(A9)}$$

On introducing thge non-dimensional time, τ, defined by equation (8), and using the fact that y, at any value of x, is simply proportional to Y, one obtains equations (7) and (9). One also finds that

$$\omega_1^2 = \frac{\pi^4}{\ell^3} \frac{EI}{M} \qquad \text{(A10)}$$

This is, of course, the "exact" result for the undamped natural frequency of a pinned-pinned shaft, since equation (1) is the corresponding exact mode shape for this case.

REFERENCES

1. Dostal, M., Roberts, J.B. and Holmes, R., "Stability Control of Flexible Shafts Supported on Oil-Film Bearings", Journal of Sound and Vibration, Vol.35, No.3, 1974, pp.361-377.

2. Dostal, M., Roberts, J.B. and Holmes, R., "The Effect of External Damping on the Vibration of Flexible Shafts Supported on Oil-Film Bearings", Journal of Sound and Vibration, Vol.51, No.1, 1977, pp.69-87.

3. Kaya, F. and Roberts, J.B., "Optimum Vibration Control of Flexible Transmission Shafts", Proceedings of the Third International Conference on Vibrations in Rotating Machinery, York, U.K. September 1984. Published by the Institution of Mechanical Engineers, London, 1984, pp.525-534.

4. Nikolajsen, J.L. and Holmes, R., "Investigation of Squeeze-Film Isolators for the Vibration Control of a Flexible Rotor", Journal of Mechanical Engineering Sciences, Vol.21, No.4, 1979, pp.247-252.

5. Roberts, J.B. and Kaya F., "Vibration Control of a Flexible Transmission Shaft by Means of a Squeeze-Film Damper: An

Experimental Investigation", to be published in the Journal of Sound and Vibration, 1986.

6. Nikolajsen, J.N., Holmes, R. and Gondhalekar, V., "Investigation of an Electromagnetic Damper for Vibration Control of a Transmission Shaft", Proceedings of the Institution of Mechanical Engineers, Vol.193, No.31, 1979, pp.331-336.

7. Haberman, H., "Le Palier Magnetique Actif 'ACTIDYNE'", AGARD Conference Proceedings, No.323, "Problems in Bearings and Lubrication", Ottawa, Canada, May 1982.

8. Ulbrich, H. and Anton,E., "Theory and Application of Magnetic Bearings with Integrated Displacement and Velocity Sensors", Proceedings of the Third International Conference on Vibrations in Rotating Machinery, York, U.K., September 1984. Published by the Institution of Mechanical Engineers, London, 1984, pp.543-552.

9. Salm, J. and Schweitzer, G., "Modelling and Control of a Flexible Rotor with Magnetic Bearings", Proceedings of the Third International Conference on Vibrations in Rotating Machinery, York, U.K., September 1984. Published by the Institution of Mechanical Engineers, London, 1984, pp.553-561.

10. Anton, E. and Ulbrich, H., "Active Control of Vibrations in the Case of Asymmetrical High-Speed Rotors by using Magnetic Bearings", Journal of Vibration, Acoustics, Stress and Reliability in Design, ASME, Vol.107, October 1985, pp.410-415.

11. Gondhalekar, V. and Holmes, R., "Design of a Radial Electromagnetic Bearing for the Vibration Control of a Supercritical Shaft", Proceedings of the Institution of Mechanical Engineers, Vol.198C,1984.

12. Jayawant, B.V., Sinha, P.K. and Aylwin, D.G., "Feedback Control Systems for d.c. Electromagnets in Passenger Carrying Vehicles", International Journal of Control, Vol. 24, No.5, 1976, pp.627-639.

13. Naslin, P., "The Dynamics of Linear and Non-linear Systems", Blackie, Edinburgh, 1965. p.244.

14. Roberts, J.B., Holmes, R. and Mason, P.J., "Estimation of Squeeze-Film Damping and Inertial Coefficients from Experimental Free-Decay Data", to be published in the Proceedings of the Institution of Mechanical Engineers, Engineering Sciences Division, U.K., 1986.

15. Ramli, M.D., Roberts, J.B. and Ellis, J., "Determination of Squeeze-Film Dynamic Coefficients from Experimental Transient Data" (to be published).

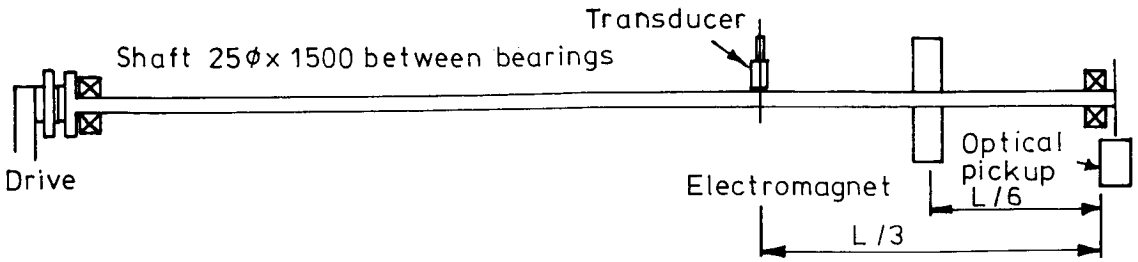

Fig 1: Layout of test rotor

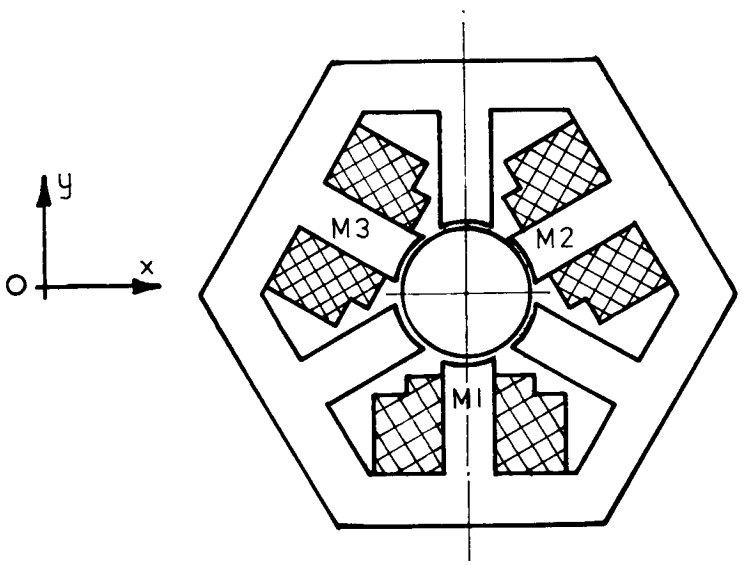

Fig 2: Configuration of electromagnet assembly

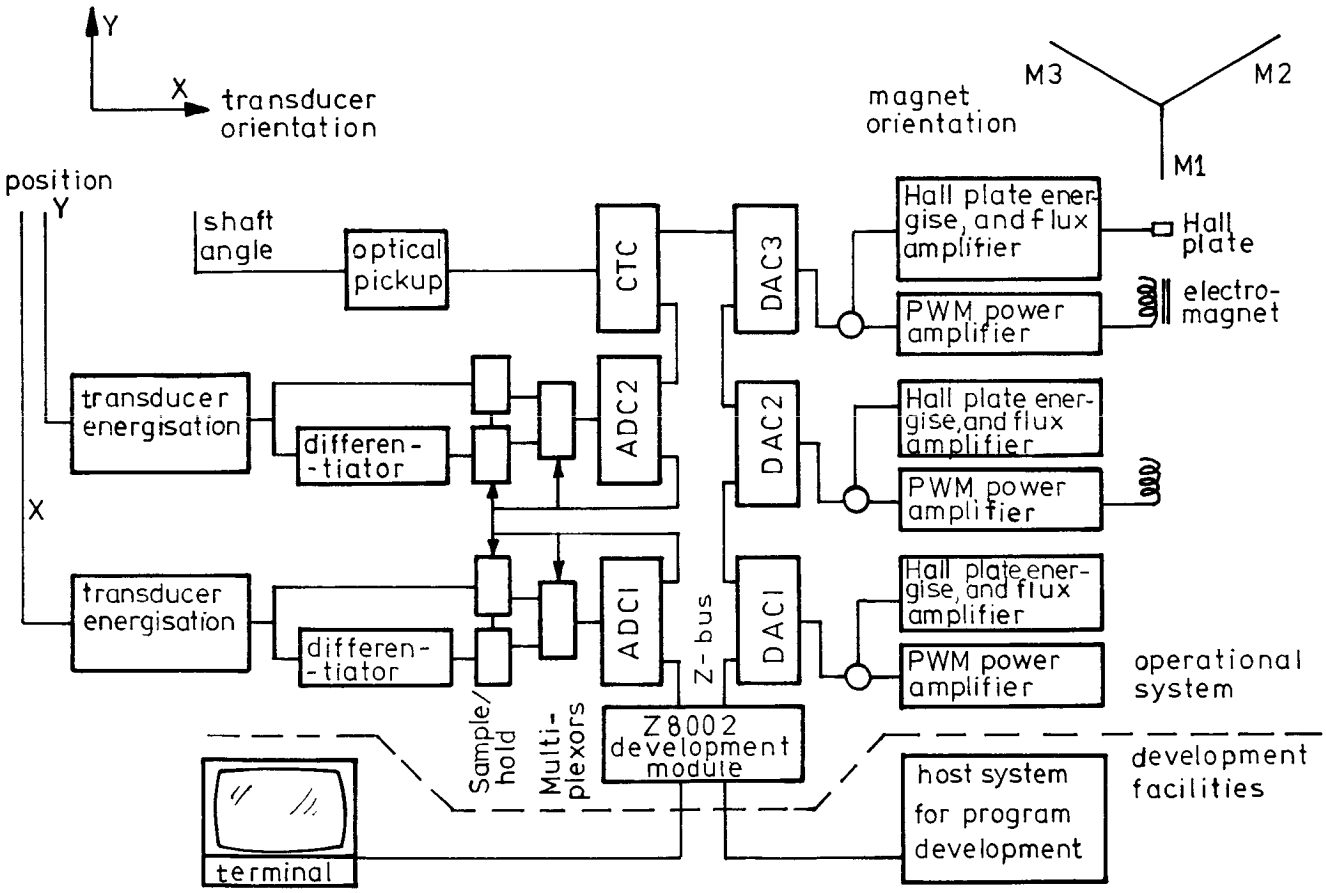

Fig 3: Schematic of electromagnet controller

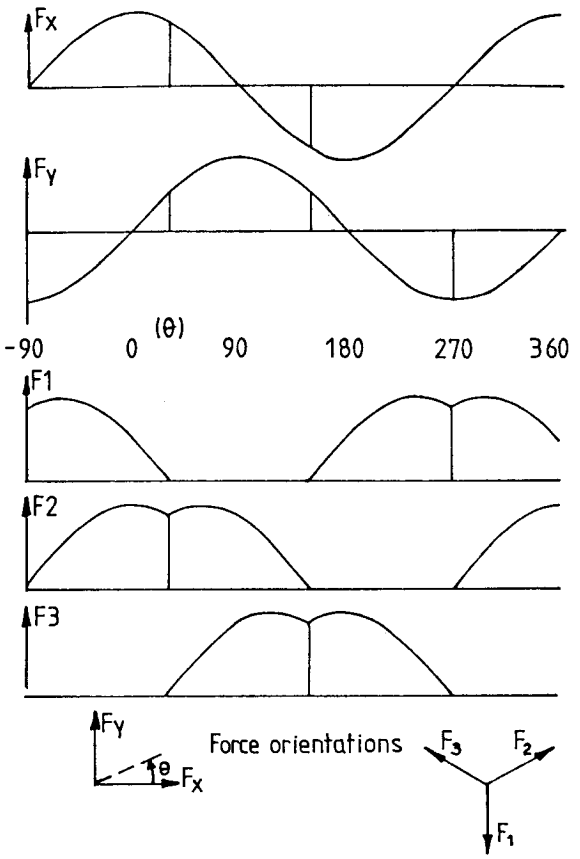

Fig 4: Waveforms of required forces along orthogonal and magnet axes.

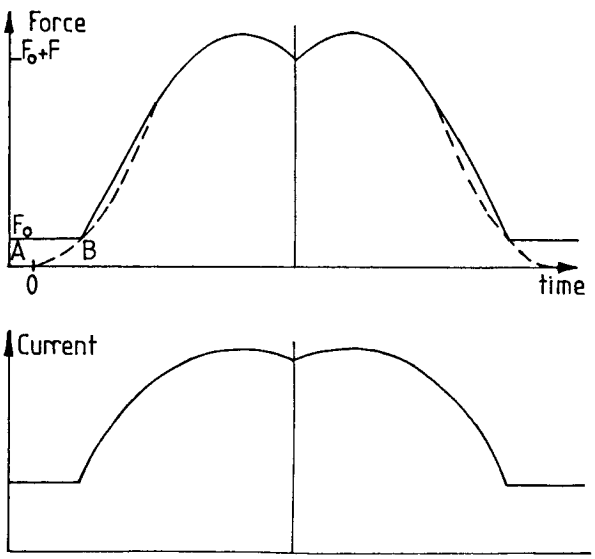

Fig 5: Effect of slew-rate limiting on current and force waveforms.

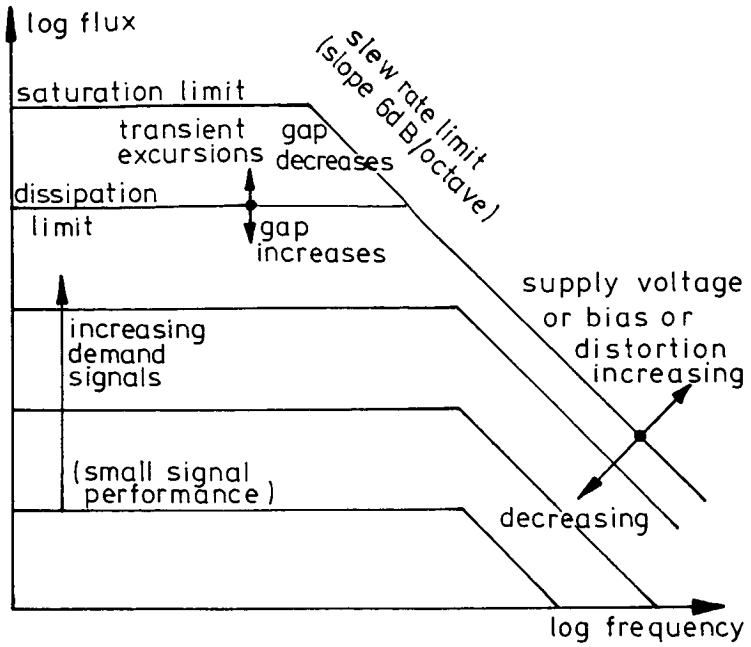

Fig 6: Performance envelope for electromagnet-power amplifier combination

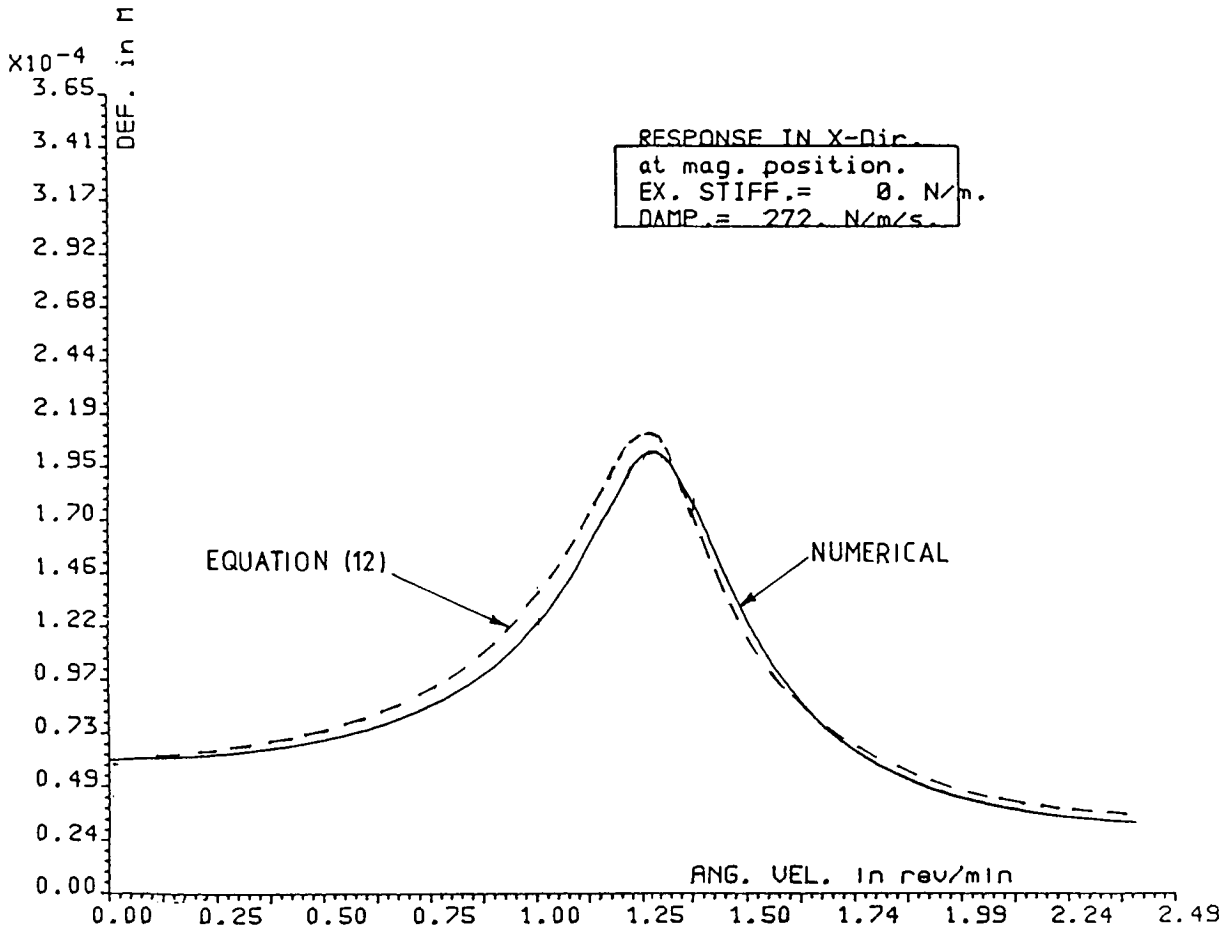

Fig 7: Predicted shaft responses

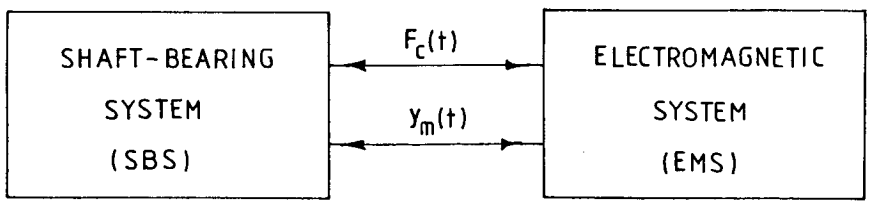

Fig 8: Mechanical and control block diagram

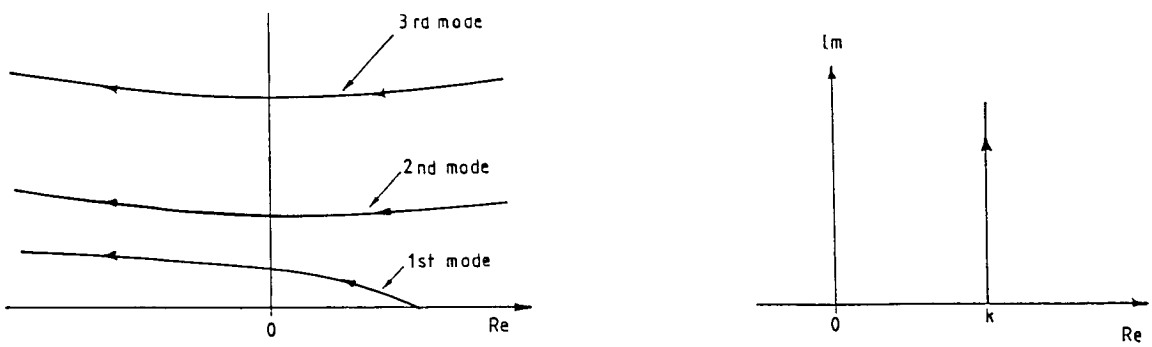

(a) SBS (b) ideal controller

Fig 9: Leonhard locus

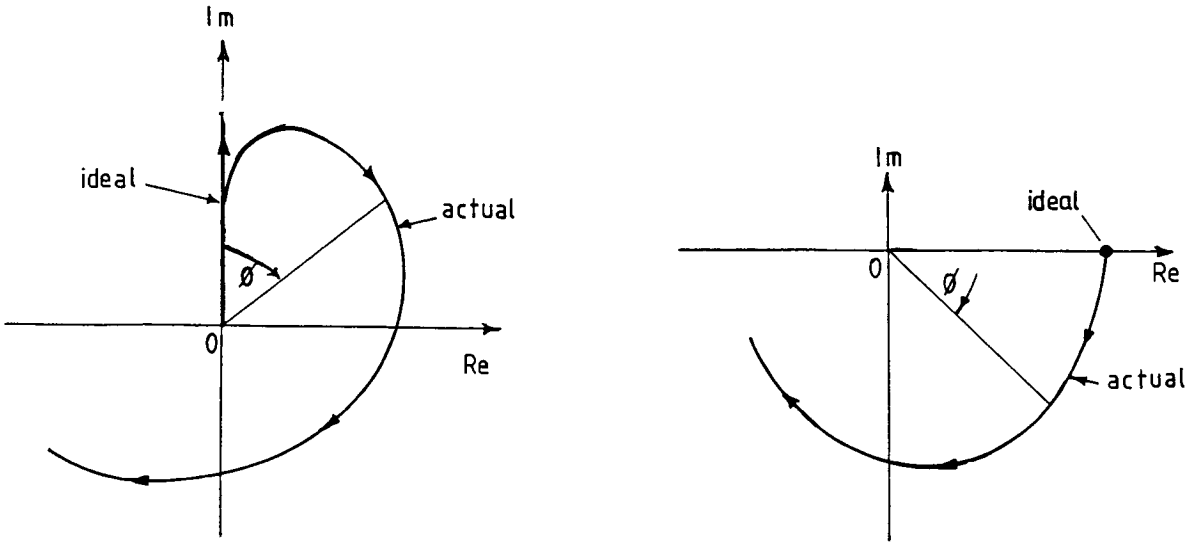

(a) damping mode

(b) stiffness mode

Fig 10: Leonhard loci for EMS

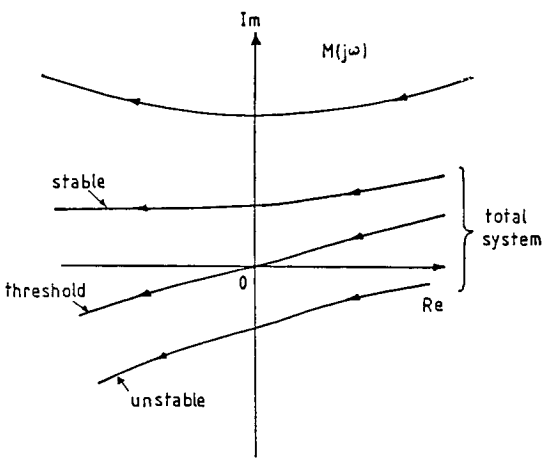

Fig 11: (right) Leonhard loci showing criteria for stability of complete system in stiffness mode

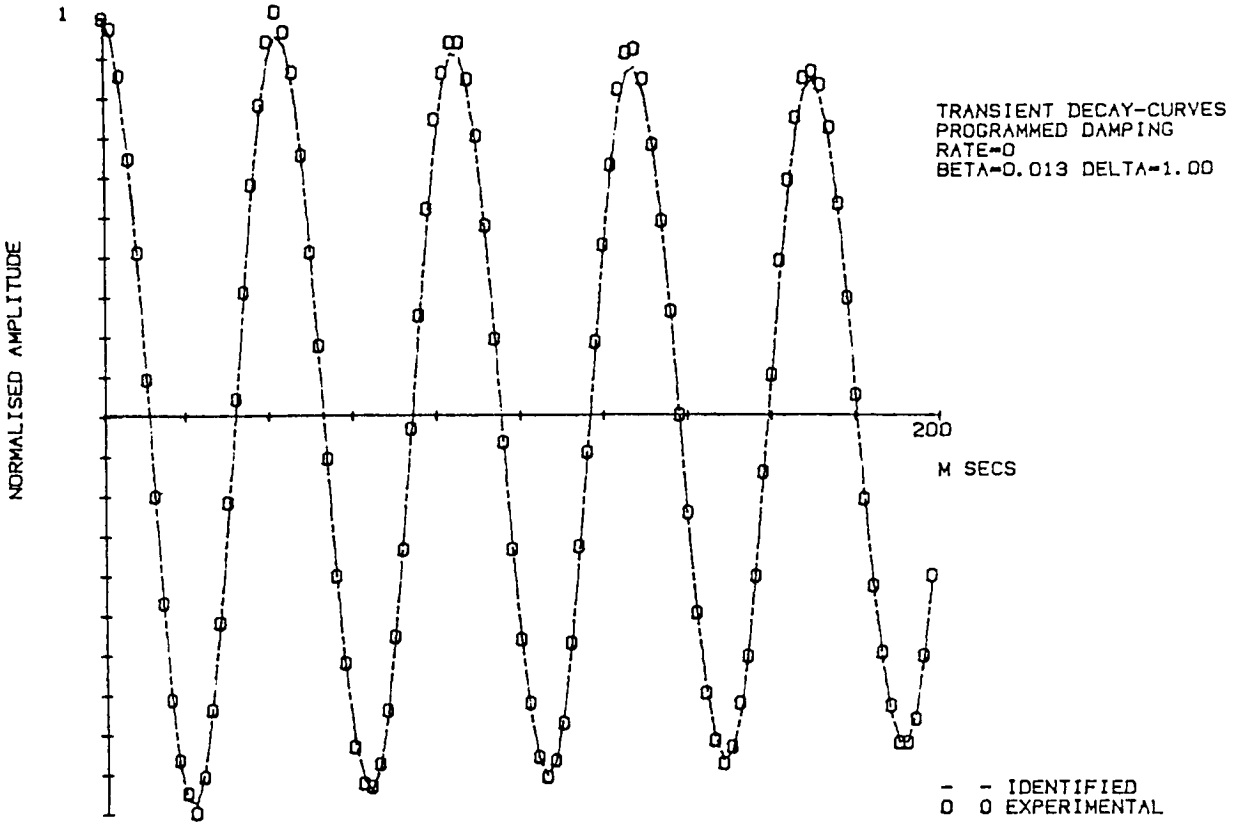

(a) controller inoperative

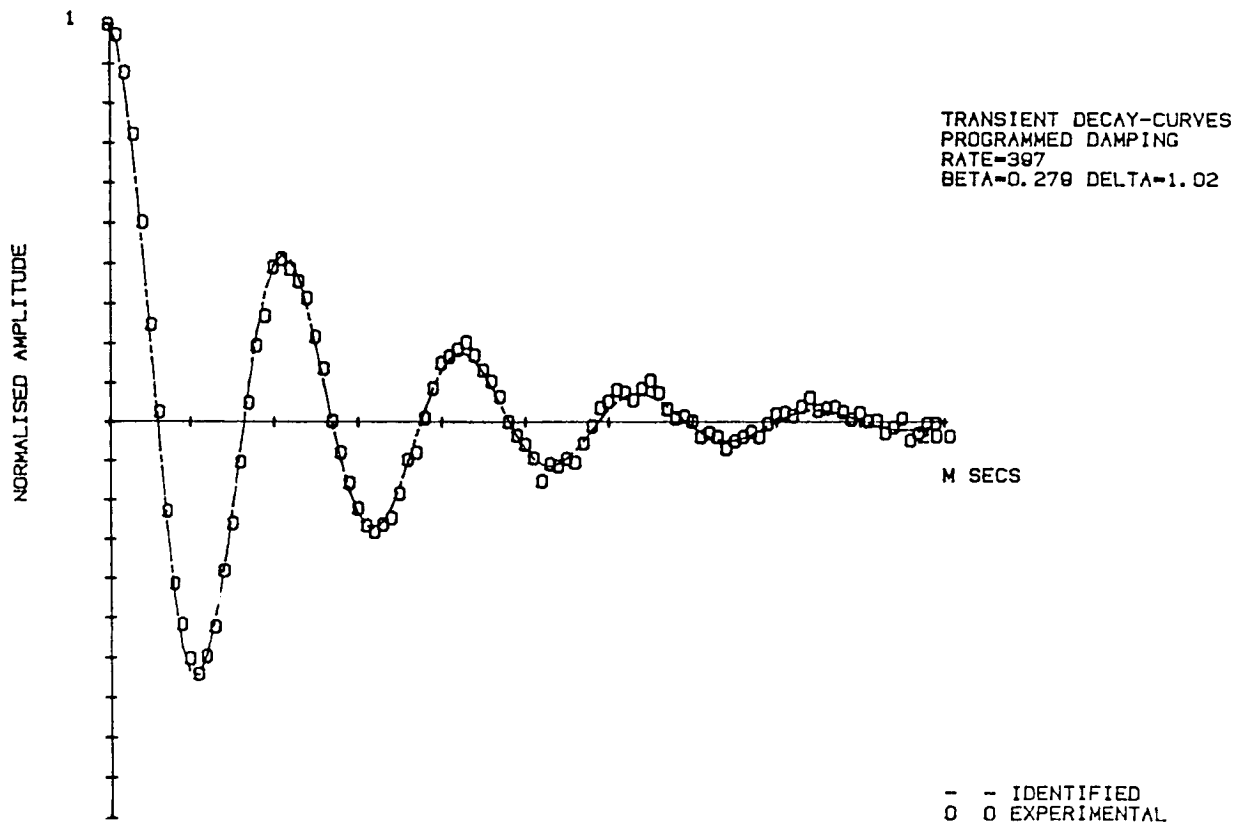

(b) with damping rate

Fig 12: Measured behaviour in free-decay tests

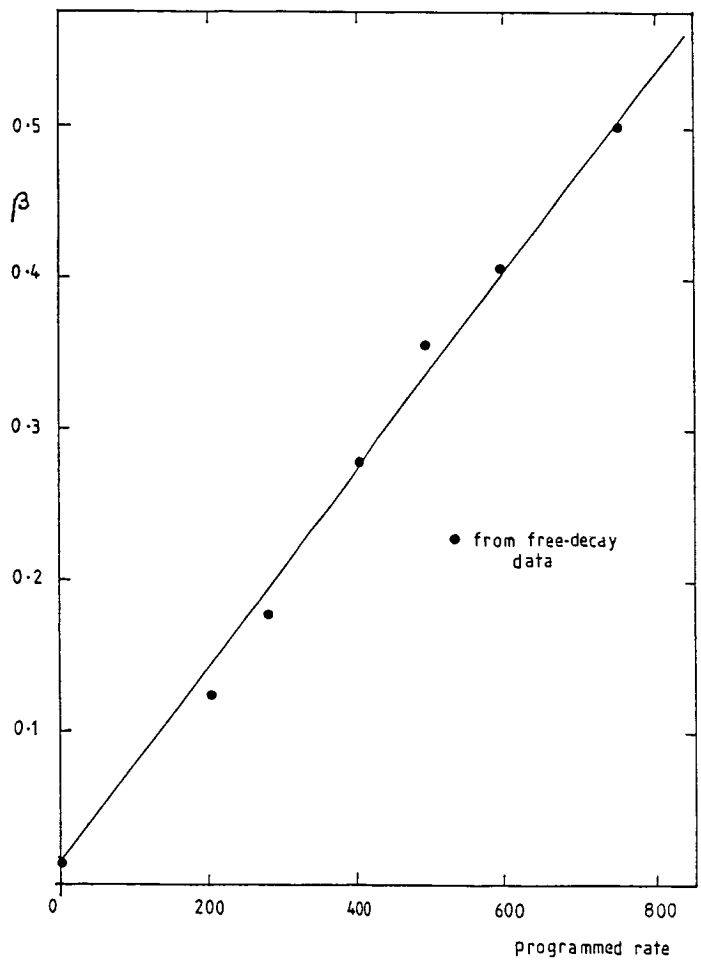

Fig 13: calibration of damping rate

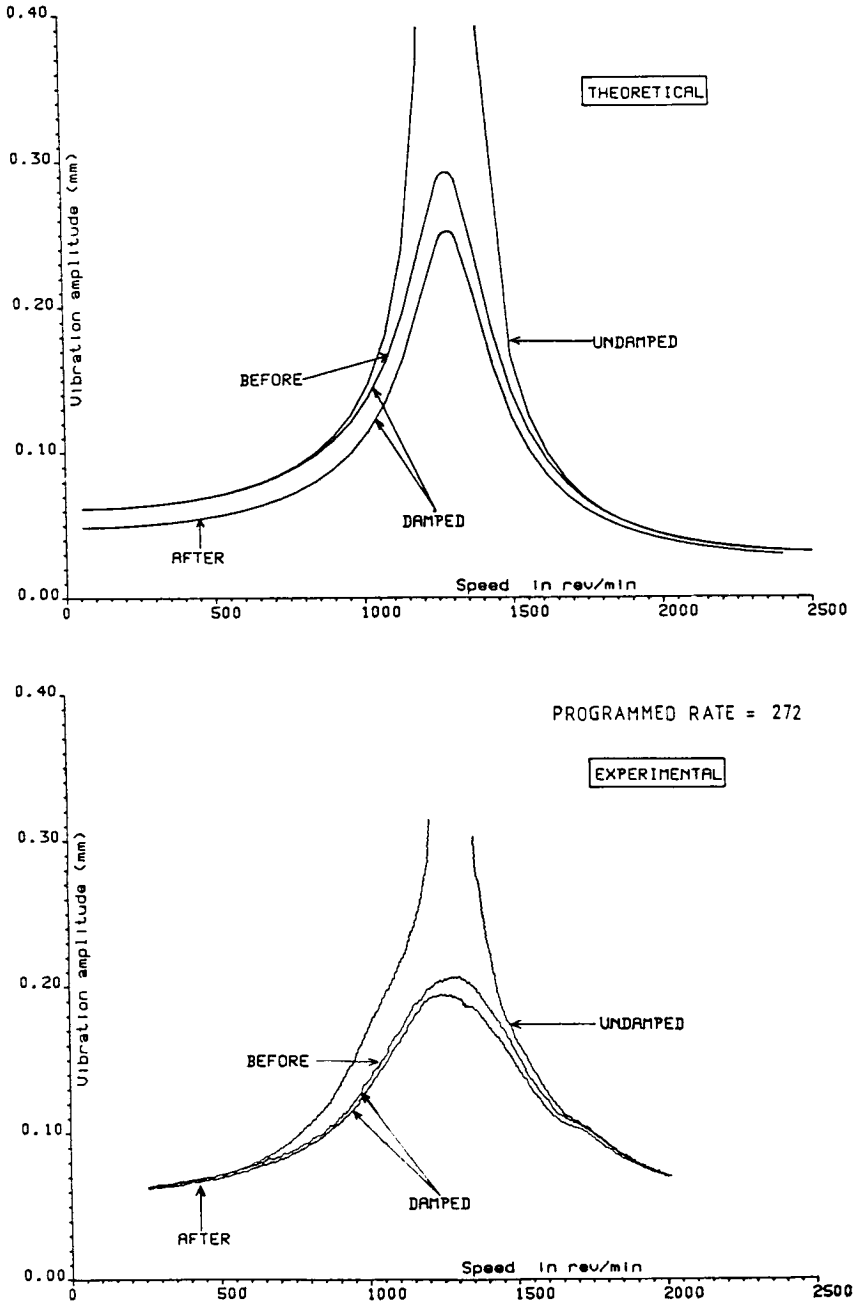

Fig 14: (a) measured and predicted responses lightly damped shaft

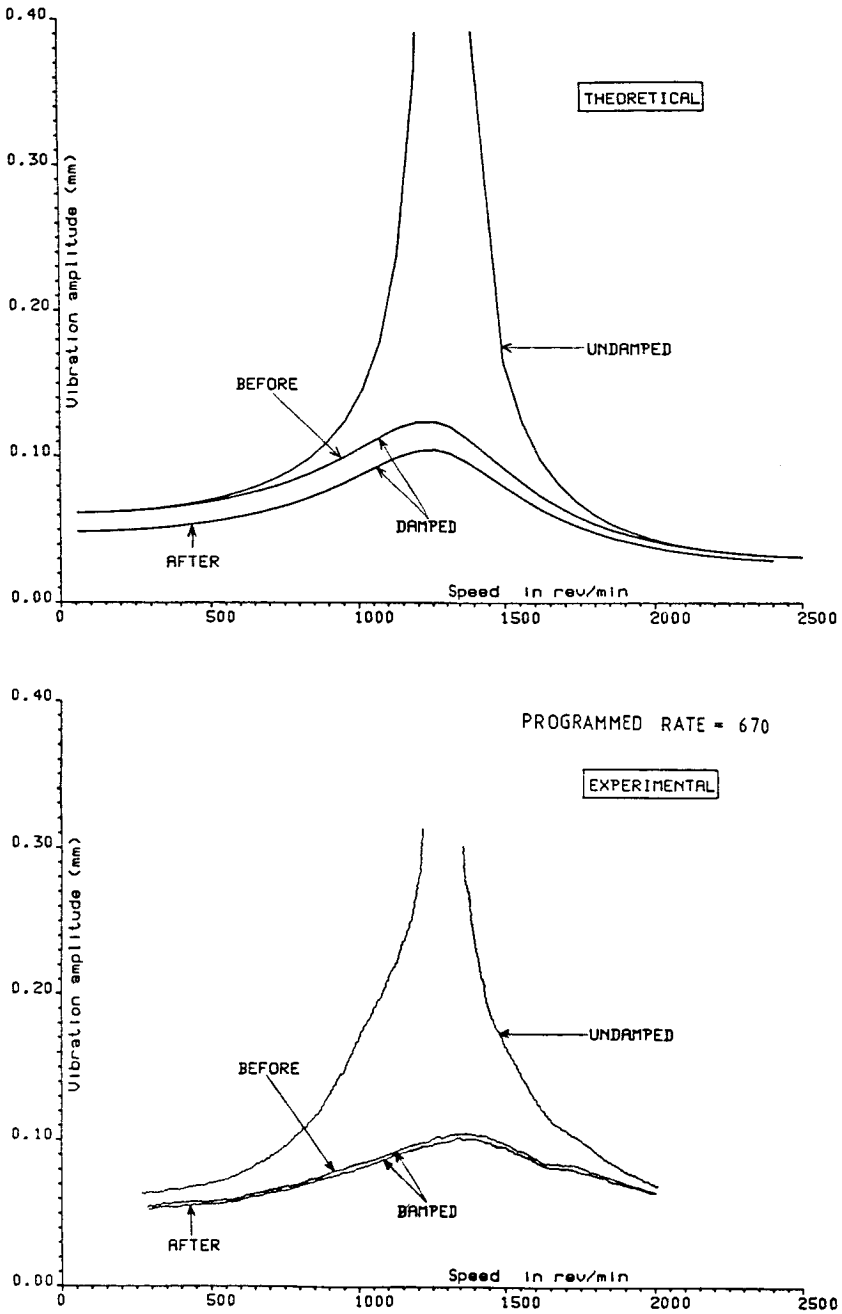

Fig 14: (b) measured and predicted responses of heavily damped shaft

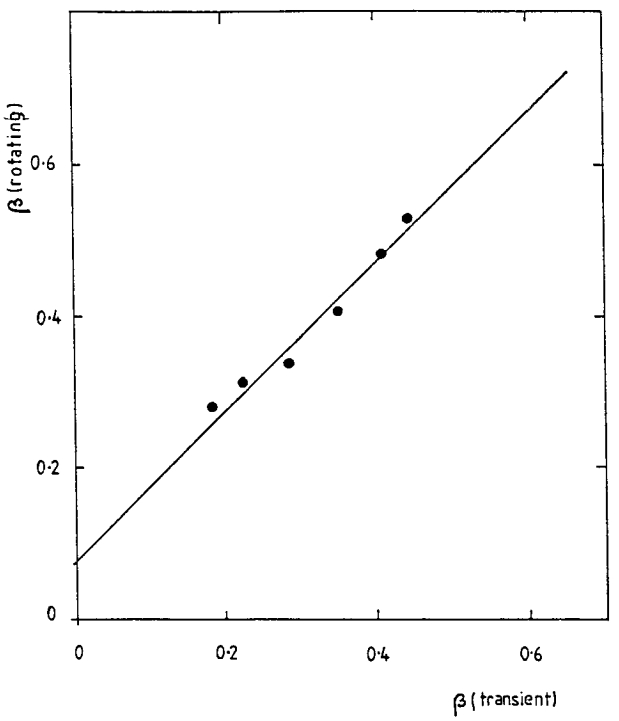

Fig 15: Comparison of damping rates from rotating and transient tests